

See discussions, stats, and author profiles for this publication at: <https://www.researchgate.net/publication/46280474>

# Constant-pH Molecular Dynamics Simulations Reveal a $\beta$ -Rich Form of the Human Prion Protein

ARTICLE in THE JOURNAL OF PHYSICAL CHEMISTRY B · OCTOBER 2010

Impact Factor: 3.3 · DOI: 10.1021/jp104753t · Source: PubMed

---

CITATIONS

48

READS

29

## 3 AUTHORS:



Sara R. R. Campos  
New University of Lisbon

13 PUBLICATIONS 122 CITATIONS

[SEE PROFILE](#)



Miguel Machuqueiro  
University of Lisbon

36 PUBLICATIONS 704 CITATIONS

[SEE PROFILE](#)



Antonio Baptista  
New University of Lisbon

91 PUBLICATIONS 2,026 CITATIONS

[SEE PROFILE](#)

# Constant-pH Molecular Dynamics Simulations Reveal a $\beta$ -Rich Form of the Human Prion Protein

Sara R. R. Campos,<sup>†</sup> Miguel Machuqueiro,<sup>†,‡</sup> and António M. Baptista<sup>\*,†</sup>

*Instituto de Tecnologia Química e Biológica, Universidade Nova de Lisboa, Av. da República, EAN, 2780-157 Oeiras, Portugal*

Received: May 24, 2010; Revised Manuscript Received: August 14, 2010

The misfolding of the prion protein (PrP) into a pathogenic  $\beta$ -rich form ( $\text{PrP}^{\text{Sc}}$ ) has been suggested to occur in the endocytic pathway, triggered by low pH. In this work we performed several constant-pH molecular dynamics simulations of human PrP 90–231 in the pH range 2–7, totaling more than 2  $\mu\text{s}$ . We observed a strong conformational pH dependence where on average the helix content decreased and the  $\beta$  content increased toward acidic pH. Unlike some proposed models, the flexible N-terminus region did not gain stable structure at low pH. Rather, the main structural changes occurred on the helix-rich C-terminus core, as proposed in other models, namely, in the regions around 135–155 and 185–200. The protonation of His187 is found to be associated with a loss of interaction between two PrP subdomains, potentially playing a major role in the misfolding process. In one of the simulations at pH 2, a stable  $\beta$ -rich structure was formed that may be an intermediate of  $\text{PrP}^{\text{Sc}}$  formation, indicating that misfolding may precede dimerization.

## Introduction

All living beings are water-based systems that depend heavily on aqueous equilibria, especially acid–base equilibrium. In particular, pH has a direct influence on the intra- and intermolecular electrostatic interactions, affecting molecular structure. This leads to the well-known pH dependence of protein structure, exemplified by protein denaturation at extreme pH values.<sup>1</sup> However, the coupling between protonation and conformation can be more subtle, as illustrated by the numerous pathologies caused by protein misfolding,<sup>2–4</sup> such as prion diseases.<sup>5</sup> In these cases, a small change in the charge state resulting from the variation of pH can induce localized conformational changes that can lead to amyloid aggregation and influence the protonation state of the protein. These examples show the importance of gaining insight into the influence of pH on protein structure and dynamics. The recently developed methods of constant-pH molecular dynamics (see ref 6 for an overview) can directly capture the protonation-conformation coupling, thereby increasing the realism of molecular dynamics (MD) simulations.

Prion diseases are rare and fatal neurodegenerative amyloid diseases that include, for instance, Creutzfeldt-Jakob disease and Gerstmann-Sträussler-Scheinker syndrome (GSS) in humans, and bovine spongiform encephalopathy in cattle. The agent responsible for this group of diseases is the prion protein (PrP), which can undergo a conformational transition from its normal cellular form,  $\text{PrP}^{\text{C}}$ , to a pathogenic and infectious *scrapie* form,  $\text{PrP}^{\text{Sc}}$ .<sup>7–9</sup>

The mature human PrP (23–231) is a glycoprotein that contains a flexible N-terminus region (23–124) followed by a globular core (125–228) composed of three  $\alpha$ -helices (HA, 144–156; HB, 174–194; HC, 200–228) and a small  $\beta$ -sheet

( $\beta$ 1, 128–131 +  $\beta$ 2, 161–164).<sup>10</sup> HB and HC are linked by a disulfide bond established between C179 and C214. The conversion of  $\text{PrP}^{\text{C}}$  into the scrapie form implies an increase of the  $\beta$ -structure (from 3 to 43%)<sup>11</sup> and a decrease of the helix content (from 42 to 30%).<sup>11</sup> This enrichment in  $\beta$ -structure is responsible for the different biochemical properties of the two isoforms: while  $\text{PrP}^{\text{C}}$  is monomeric, soluble, and protease K sensitive,  $\text{PrP}^{\text{Sc}}$  forms insoluble fibrillar aggregates that are protease K resistant.<sup>7–9</sup> The insolubility of  $\text{PrP}^{\text{Sc}}$  has hindered researchers from determining its detailed structure.<sup>11–13</sup>

According to the “protein-only hypothesis”,  $\text{PrP}^{\text{Sc}}$  can act as template in the misfolding of  $\text{PrP}^{\text{C}}$ , being the sole infectious agent.<sup>9,14</sup> On the other hand, the mechanism that triggers the spontaneous conversion of  $\text{PrP}^{\text{C}}$  into  $\text{PrP}^{\text{Sc}}$  remains elusive. It has been suggested, however, that the conversion occurs in the endocytic pathway triggered by low pH.<sup>8,15–18</sup> In fact,  $\text{PrP}^{\text{C}}$  has been shown to cycle between the cell surface and endocytic compartments,<sup>19,20</sup> while  $\text{PrP}^{\text{Sc}}$  formation has been related to the endocytic pathway.<sup>21–23</sup> In addition, it has been observed that acidic pH induces the formation of  $\beta$ -sheet, under mildly denaturing conditions,<sup>15,16,24–28</sup> or even under “native” conditions.<sup>5</sup> Moreover, NMR structures of the globular part of human PrP at pH 4.5 and pH 7.0<sup>10,29</sup> show the same global fold (indicating that  $\text{PrP}^{\text{C}}$  is metastable at low pH<sup>5</sup>) but with local differences, especially in  $\beta$ 2 and in the C-terminus regions of HA and HB.

Because of the difficulty of experimentally determining the structure of  $\text{PrP}^{\text{Sc}}$ , MD simulations can be particularly useful to study PrP misfolding. However, most MD simulations of PrP only detected small structural changes despite the use of the most varied strategies to create instability, which included: high temperatures,<sup>30–33</sup> disease related point mutations,<sup>30,32,34,35</sup> hydrophobic environment ( $\text{CCl}_4$ )<sup>35</sup> and low pH.<sup>18,31,33,36–39</sup> Nonetheless, Shamsir and Dalby<sup>32</sup> were able to observe the formation of new  $\beta$ -sheets in the globular region of D178N mutants at 500 K, while Daggett and co-workers have observed the elongation of the  $\beta$ -sheet and the formation of new  $\beta$ -structure in the N-terminus region at low pH.<sup>34,36,37</sup> MD simulations

\* To whom correspondence should be addressed. E-mail: baptista@itqb.unl.pt. Phone: +351-21-4469619. Fax: +351-21-4411277.

<sup>†</sup> Instituto de Tecnologia Química e Biológica, Universidade Nova de Lisboa, Av. da República, EAN, 2780-157 Oeiras, Portugal.

<sup>‡</sup> Current address: Centro de Química e Bioquímica, Faculdade de Ciências da Universidade de Lisboa, 1749-016 Lisboa, Portugal.

performed at acidic pH observed a decreased structural stability, particularly in HA<sup>36–39</sup> and in the C-terminus region of HB.<sup>18,31,38</sup>

Most experimental assays, including studies of pH-dependent misfolding,<sup>5,15,25,26,28</sup> use the segment 90–231 that corresponds to the protease K resistant core of PrP<sup>Sc</sup>.<sup>7</sup> In particular, the 90–124 region is thought to acquire structure during the transition to the scrapie form, with studies showing that epitopes in the 90–120 region of PrP<sup>C</sup> become inaccessible in PrP<sup>Sc</sup>.<sup>40</sup> For this reason, the segment 90–231 is probably the most relevant one for misfolding studies.

In this work we used the stochastic titration method<sup>6,41–44</sup> to perform constant-pH MD simulations of human PrP 90–231. Several groups in the protein are titratable in the acidic range of endosomes (pH 4–7<sup>45</sup>), which means that different protonation states can coexist. The constant-pH MD method allowed to sample these protonation states and it was effective in capturing the global effects of the protonation-conformation coupling. To our knowledge, this was the first time that constant-pH MD simulations were performed on a prion.

## Methods

**Construction of Human PrP 90–231 Structure.** We began the simulations from four different constructs of human PrP 90–231. Since the available NMR structures contained only the segment 125–228, it was necessary to add the remaining residues. The NMR structure belonging to the Syrian hamster, 2PRP,<sup>46</sup> is the only PrP structure in the protein data bank that has the 90–124 segment. By use of a similar approach to the one of DeMarco and Daggett,<sup>39</sup> we grafted this segment of 2PRP onto the human PrP structure. The residues 229–231 were inserted using PyMOL 0.99 (<http://www.pymol.org>). This software was also used to mutate Asp97 of hamster PrP to the corresponding Ser in human. The selected NMR structures of the human PrP were 1QM0<sup>29</sup> and 1HJM,<sup>10</sup> obtained at pH 4.5 and pH 7, respectively; as noted in the Introduction, these two structures are very similar and correspond to PrP<sup>C</sup>, which is metastable at low pH.<sup>5,10</sup> The structures selected from 2PRP were the two with the least secondary structure in the 90–124 segment, according to DSSP criterion.<sup>47</sup> Combining these two structures (90–124) with 1QM0 and 1HJM, we built the four aforementioned starting structures. The N-terminus was capped, and the disulfide bond was kept intact.

**Constant-pH MD Simulations.** The constant-pH MD method used was the implementation for the GROMACS package of the stochastic titration method developed by Baptista and co-workers.<sup>6,41–44</sup> The stochastic titration method consists essentially of a piecewise molecular mechanics/molecular dynamics (MM/MD) simulation in which the protonation states of the protein are periodically replaced with new (eventually identical) states obtained at the end of a Monte Carlo (MC) simulation using free-energy terms derived from Poisson–Boltzmann (PB) calculations on the instantaneous protein conformation. The constant-pH MD simulations were performed at pH of 2, 4, 5, 6, and 7 (the pH of endosomes is in the range 4–7<sup>45</sup>). For each starting structure and pH, three replicates were done by randomizing initial velocities, amounting to a total of 12 simulations per pH value. The simulations were 40 ns long at pH 2 and 4 and 30 ns at the other pH values. This amounts to a total of 2.04  $\mu$ s of simulation time. Structures were saved every 2 ps. At pH 4, 5, and 6 we titrated the histidines and all carboxylic acids, at pH 7 only the histidines, and at pH 2 only the carboxylic acids. We also considered proton isomerism for each titrable site.<sup>48</sup> The reduced titration approach<sup>6</sup> was used to reduce the computational cost. Every 50 cycles, a complete

titration was performed and the titrable sites list updated. The threshold used to exclude a site from the list was 0.999 relative frequency in a given state. Each constant-pH MD cycle was 2 ps long, and each solvent relaxation period lasted for 0.2 ps.

**PB/MC Settings.** The software used for the PB calculations was the MEAD package (version 2.2.0).<sup>49</sup> The atomic charges and radii were taken from the GROMOS96 53A6 force field.<sup>50</sup> The molecular surface was defined by a rolling probe of radius 1.4 Å, and the Stern layer was 2 Å. The dielectric constant was 2 in the molecular interior and 80 in the solvent. The PB calculations were done employing the finite difference method with a focusing procedure,<sup>51</sup> using grid spacings of 1.0 and 0.25 Å. The temperature was 310 K, and the ionic strength was 0.15 M. The MC simulations were done with the program PETIT (version 1.5)<sup>48</sup> performing  $10^5$  MC steps for each calculation. Each step consisted of a cycle of random choices of state (including tautomeric forms) for all individual sites and for pairs of sites with a coupling above 2.0 pK<sub>a</sub> units,<sup>48,52</sup> whose acceptance/rejection followed a Metropolis criterion.<sup>53</sup>

**MM/MD Settings.** The MM/MD simulations were performed using GROMACS 3.2.1<sup>54,55</sup> and the GROMOS96 53A6 force field.<sup>56</sup> Each starting structure was put in a rhombic dodecahedron box with periodic boundary conditions and solvated with SPC water molecules.<sup>57</sup> The boxes had different sizes, containing between 16089 and 19794 water molecules. Nonbonded interactions were treated using a twin-range cutoff of 8/14 Å and updating the neighbor lists every 10 fs. Long-range electrostatics were treated using a generalized reaction field,<sup>58</sup> with a dielectric constant of 54 and an ionic strength of 0.15 M. Solvent and solute were separately coupled to temperature baths at 310 K using Berendsen coupling<sup>59</sup> with a relaxation time of 0.1 ps. The Berendsen coupling was also used to keep the pressure at 1 bar, with a relaxation time of 0.5 ps and an isothermal compressibility of  $4.5 \times 10^{-5}$  bar<sup>-1</sup>. All bonds were constrained using the LINCS algorithm.<sup>60</sup> Before starting the constant-pH MD simulations the structures were submitted to a three-step energy minimization. First the steepest descent algorithm was used for  $10^4$  steps, without constraints but applying position restraints (100 kJ mol<sup>-1</sup> nm<sup>-2</sup>) on the heavy atoms. Then this procedure was repeated without position restraints and with all bonds constrained. Finally, the low-memory Broyden–Fletcher–Goldfarb–Shanno algorithm was used during  $10^4$  steps. After the energy minimization, the structures were equilibrated during 50 ps of MD, with constant volume and position restraints (1000 kJ mol<sup>-1</sup> nm<sup>-2</sup>) on all atoms. This equilibration procedure was repeated with only the C- $\alpha$  atoms restrained.

**Analyses.** The equilibrated last 20 ns of each simulation were used for analysis. Secondary structure assignment was done using the DSSP program by Kabsch and Sander.<sup>47</sup> The  $\beta$ -content includes all residues assigned to  $\beta$ -sheet or  $\beta$ -bridge, the helix-content includes all types of helix, and helicity refers to the fraction of residues in helix. Other analyses were performed using either the GROMACS package<sup>54,55</sup> or in-house tools. The calculation of correlation-corrected statistical errors for averages (elsewhere referred to as “errors”) was done using standard methods.<sup>61</sup> The pK<sub>a</sub> of each titrable site was calculated from the averaged occupancies ( $f$ ) at each pH value after fitting the data to the Hill equation

$$f(\text{pH}) = [1 + 10^{n(\text{pH} - \text{pK}_a)}]^{-1} \quad (1)$$

where  $n$  is the Hill coefficient, also calculated from the fit. The fits were done using the nonlinear least-squares Marquardt–Levenberg

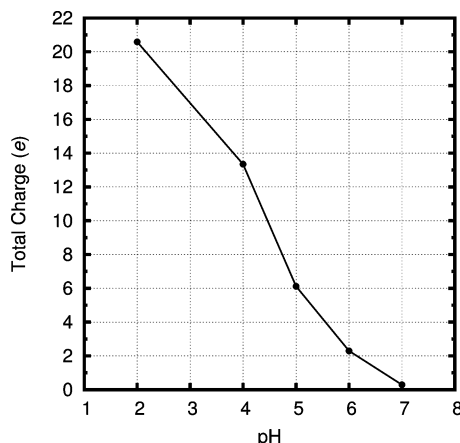


**Figure 1.** Titration curve obtained from the constant-pH MD simulations of human PrP 90–231. The errors of the average charges are smaller than 0.14  $e$ .

**TABLE 1: Calculated  $pK_a$  Values<sup>a</sup>**

residue	$pK_a$
Asp-144	3.74 ± 0.03
Asp-147	3.50 ± 0.15
Asp-167	3.97 ± 0.02
Asp-178	3.68 ± 0.11
Asp-202	3.43 ± 0.22
Cter (Ser-231)	3.47 ± 0.06
Glu-146	4.33 ± 0.11
Glu-152	4.30 ± 0.06
Glu-168	4.44 ± 0.07
Glu-196	4.12 ± 0.08
Glu-200	4.21 ± 0.01
Glu-207	4.69 ± 0.10
Glu-211	4.83 ± 0.05
Glu-219	4.77 ± 0.03
Glu-221	4.32 ± 0.05
His-96	5.50 ± 0.12
His-111	5.47 ± 0.19
His-140	5.88 ± 0.03
His-155	5.13 ± 0.13
His-177	5.97 ± 0.28
His-187	4.72 ± 0.11

<sup>a</sup> The indicated statistical errors correspond to the normal-asymptotic standard errors associated with the fit to eq 1.<sup>62</sup>

algorithm<sup>62</sup> implemented in gnuplot 4.0 (<http://www.gnuplot.info>), weighting the average protonations with their errors.

## Results

**$pK_a$  Measurements.** Figure 1 represents the total titration curve of human PrP 90–231 obtained from the simulations by calculating the average net charge at each pH value. Table 1 lists the computed  $pK_a$  of each titratable site (see details in Methods). Unfortunately there are no experimental results to compare to ours, though Langella et al.<sup>38</sup> had already used a rigid molecule PB/MC model to calculate the  $pK_a$  values of the titratable residues in region 125–228 of human PrP. In that study the authors point out that His155 and His187, which have the smallest  $pK_a$  values among the histidines, are also involved in conformational rearrangement upon protonation. We also observed those histidines to have the smallest  $pK_a$  values, being the His187  $pK_a$  particularly low. As will be seen below, this residue is located in a very flexible region of human PrP (185–200) where a significant pH-dependent conformational rearrangement takes place. In addition, the mutation H187R has been associated with GSS.<sup>63</sup> These

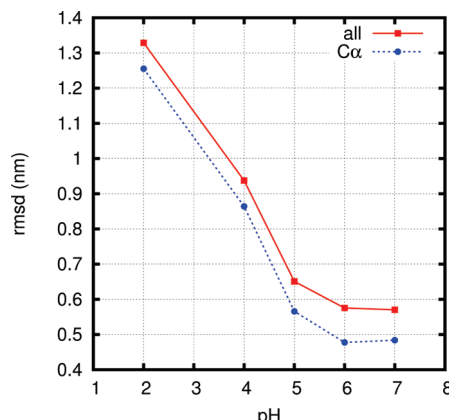


**Figure 2.** Average rmsd from the initial NMR structure of the globular part (125–228) of PrP at each pH value. The rmsd values were calculated relative to the initial NMR structure of the respective simulation, which was either 1QM0 or 1HJM, as described in detail in the Methods section. The fitting of the structures considered only the C- $\alpha$  atoms and mass-weighted rmsd was calculated using all atoms (all) or C- $\alpha$  atoms (C $\alpha$ ). The errors of the average rmsds are smaller than 0.013 nm.

results suggest that His187 may play an important role in the conformational stability of PrP, which is investigated below in more detail.

**pH Effect on the Overall Structure.** There is an obvious variation of human PrP structure with pH, as can be seen in the root-mean-square deviation (rmsd) plot in Figure 2. Lowering the pH increased on average the deviation from the initial structure, implying a pH-dependent conformational change. The average number of H-bonds in the main chain decreases at low pH values suggesting that these structural modifications are associated with a loss of secondary structure (Figure 3a).

By looking at the radius of gyration and the solvent accessible surface area (Figure 3b), we can conclude that the shape of the globular core changes in a pH-dependent way, adopting the most compact conformation at pH 5.

To see where those conformational changes were taking place, we calculated the average structure at each pH, represented in Figure 4. We can see that the regions that change the most with pH are HA and the C-terminus of HB. These changes are mainly characterized by a loss of helical structure.

In addition, to identify the more flexible regions, we calculated the root-mean-square fluctuation (rmsf) along the sequence, for each pH value (Figures 4 and 5). In perfect agreement with previous observations, the regions with the highest rmsf are those already reported to show flexibility in NMR experiments: (1) the N-terminus region;<sup>10,29,64</sup> (2) HA up to  $\beta$ 1;<sup>64</sup> (3) the loop between  $\beta$ 2 and HB;<sup>10,65</sup> (4) C-terminus of HB up to HC;<sup>10,64</sup> (5) C-terminus of HC.<sup>64</sup> The most stable structural elements (smaller rmsf) are: N-terminus of HB, central part of HC, and the  $\beta$ -sheet ( $\beta$ 1+ $\beta$ 2).

The protein shows the highest fluctuations at pH 2, suggesting a gain of plasticity at low pH values. The regions where the fluctuations vary the most with pH are the region from HA up to  $\beta$ 1 (135–155) and the region from C-terminus of HB up to HC (185–200). These are the same regions that, on average, change the most with pH (Figure 4), suggesting that a gain of plasticity may be responsible for the conformational changes that occur at low pH. Curiously, pH 6, and not pH 7, is the pH where the smallest fluctuations are observed, showing a curve that is almost always below pH 7, with the exception of the C-terminus end. Furthermore, pH 7 presents significant fluctua-

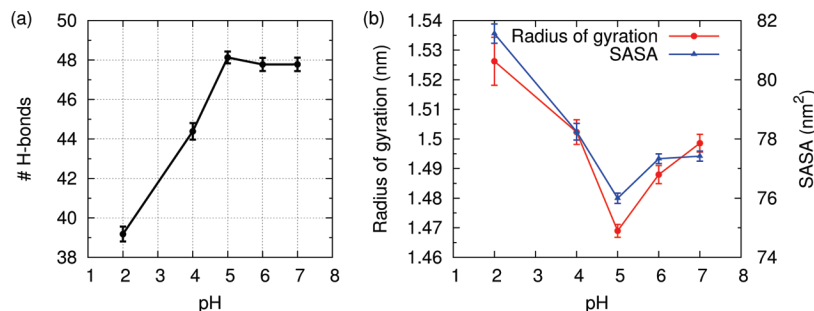


**Figure 3.** (a) Average number of H bonds in the main chain of PrP at each pH value. (b) Average radius of gyration and solvent accessible surface area (SASA) of the globular part (125–228) of PrP at each pH value.

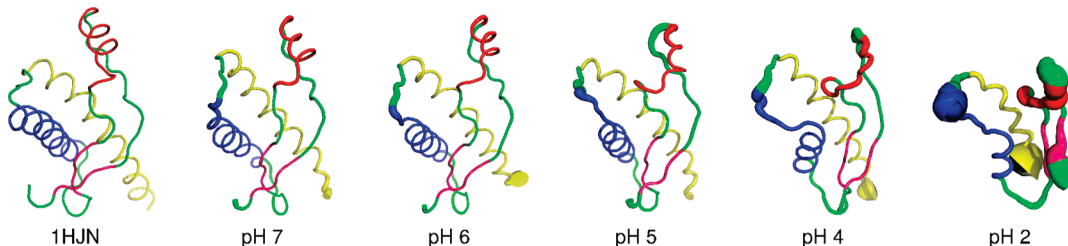


**Figure 4.** Average structure at each pH value. The thickness of the coil represents the fluctuations of the heavy atoms around the average structure. On the left, is shown the average structure from the 1HJM set of structures,<sup>10</sup> of which 1HJM is the most representative. For clarity, only the globular part (125–228) is represented. Color code: pink is region 128–131 + 161–164 ( $\beta_1 + \beta_2$ ); red is region 144–156 (HA); blue is region 173–194 (HB); yellow is region 200–228 (HC). The molecular representation was done with PyMOL 0.99 (<http://www.pymol.org>).

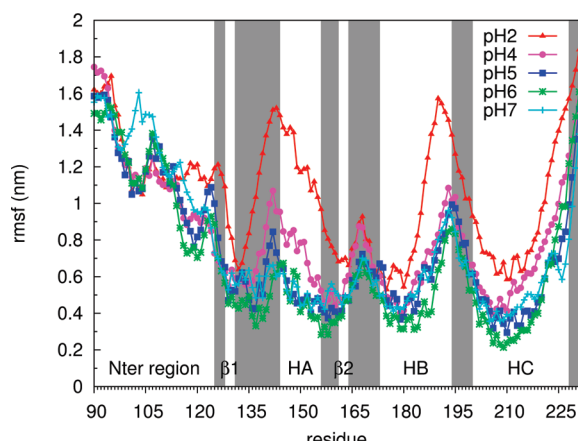


**Figure 5.** rmsf of each residue at each pH value. All heavy atoms were considered in the rmsf calculations, but very similar curves were obtained when using only the backbone atoms. Nter, N-terminus.

tions in the N-terminus region, whose flexibility does not seem to be much affected by pH.

**Role of His187 in the Conformational Rearrangement of PrP.** As noted above, His187 may play a role in the pH-induced structural rearrangement of PrP, in agreement with simulation studies<sup>38</sup> and the fact that the H187R mutation was related with GSS.<sup>63</sup> In particular, the  $pK_a$  of 4.72 here computed for His187 is compatible with its involvement in a conformational rearrangement triggered at endosomal pH. To investigate this potential role in more detail, we performed an analysis of the interactions of the His187 titrable side-chain with other protein residues. Figure 6 shows how the protonation (charging) of His187 leads to the loss of many of its main interactions and to the gain of some new ones. A large part of the lost interactions, mainly with Arg156, Asn159, and Gln160, occurs at the C-terminal of HA and at the loop between HA and  $\beta_2$ , which are regions experiencing large pH-induced structural rearrangements and fluctuations (Figures 4 and 5). Furthermore, His187 is itself part of the 185–200 segment, which also displays

extensive pH-dependent rearrangements and fluctuations (Figure 4 and 5), and its protonation leads to a change of the interactions within this region, especially the formation of new interactions with Glu196 and Asp202. When a similar analysis of the His187 interactions is done along descending pH values, we obtain, as expected, a gradual transition from the “neutral” to the “charged” interaction trends shown in Figure 6 (see the Supporting Information). Such strongly protonation-dependent interactions were not observed for the other histidine residues.

These results suggest that His187, being at the interface between the  $\beta_1 + \text{HA} + \beta_2$  and HB + HC subdomains, may play a role in their mutual anchorage when it is in the neutral form. As the pH is lowered, the charged form of His187 may be better stabilized by the solvent, leading to a weaker contact between these two subdomains and allowing the occurrence of large structural fluctuations and rearrangements. The role of this intrasubdomain interaction in prion misfolding has been previously suggested based on experimental and computational evidence (see refs 66 and 67 and references therein) and seems to be supported by our results.

**pH Effect on the Secondary Structure.** An evident feature in Figure 4 is the loss of helical structure with pH decrease. Figure 7 shows to what extent the average helix content changes with pH. There is a gradual decrease of total helicity with acidification, being at pH 2 almost half the value observed at pH 7. The trend is similar in each of the three regions corresponding to HA, HB, and HC (Figure 7b). Still, HA showed to be the least stable helix, being the one losing more helix content and more abruptly with pH, while HC was the most stable one, losing less structure. Therefore, the stability of these helices seems to be somewhat a consequence of their sizes, as would be expected from the cooperative effect of their hydrogen bonds. In addition, the disulfide bridge between HB and HC should also stabilize these two helices to some extent.

Inspection of Figure 4 also suggests a gain of  $\beta$ -like structure. For this reason, we calculated the average  $\beta$  content, in the globular core, at each pH (inset of Figure 8a). Although it does not vary as markedly as the helix content, a clear trend of  $\beta$

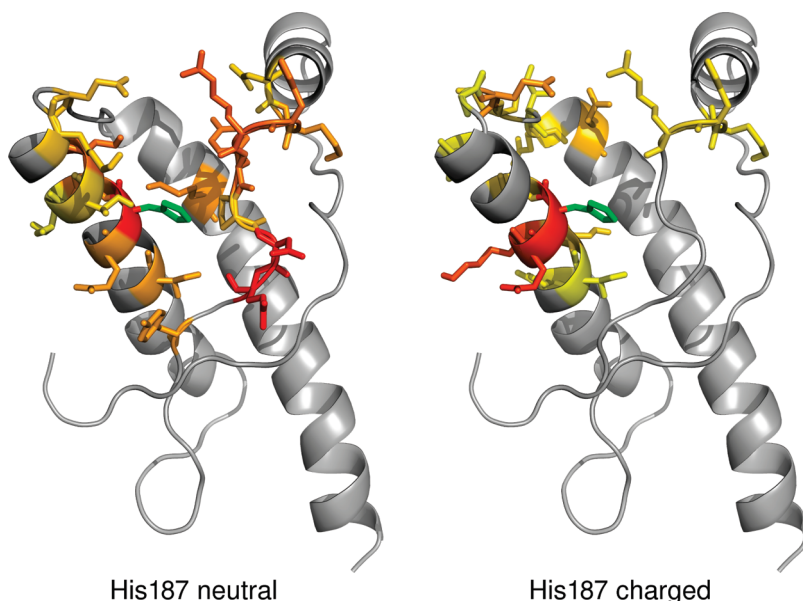


**Figure 6.** 1HJM NMR structure showing the residues with which His187 (in green) interacts when it is neutral (left) or charged (right). The fraction of interactions observed with each residue is mapped using a yellow (lowest) to red (highest) color gradient. The fractions were computed using the conformations from the simulations at all pH values and are normalized relative to the corresponding total number of interactions, so that the gradient colors are directly comparable between both images. Only residues with a fraction of interactions above 0.005 are shown. His187 is considered to interact when one of its side-chain nitrogens is at most at 0.35 nm from an oxygen, nitrogen or sulfur atom of the protein.

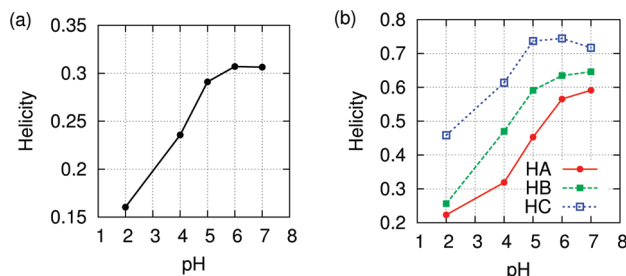


**Figure 7.** Average helicity as a function of pH. (a) Total helicity calculated over the total number of residues (142). The errors of the average helicity are smaller than 0.003. (b) Helicity in the regions corresponding to HA (144–156), HB (173–194), and HC (200–228). The helicity fraction is calculated over the size of each region (HA, 13; HB, 22; HC, 29). The errors of the average are smaller than 0.016 for HA, 0.012 for HB, and 0.009 for HC.

content increase can be seen with pH reduction. We also compared the histograms of the  $\beta$  content, in the globular core, at each pH (Figure 8a). All curves, with the exception of pH 6, show a peak at 8 residues corresponding to the original  $\beta$ -strands ( $\beta_1 + \beta_2$ ). The loss of some  $\beta$ -structure gives rise to the peaks at 4 and 6 residues, but the original  $\beta$ -sheet piece only in very rare cases completely disappears, as we can verify by the absence of any peak at 0 residues. At pH 6, unlike the other pH values, the most frequent case corresponds to only 4 residues in  $\beta$ -structure. However, the tails in these plots are even more interesting than the peaks. Upon close inspection of the region corresponding to 12 or more residues, we can distinctly see that lower pH values are favoring the occurrence of structures richer in  $\beta$ -structure. At pH 2, there are structures with as much as 37 residues in  $\beta$ . So, not only the helix structure is being lost at low pH but also the formation of new  $\beta$ -sheet is being favored.

To determine if new  $\beta$ -sheet could also be forming in the N-terminus region of PrP, we did a similar analysis considering only this part of the protein (Figure 8b). Though it may transiently form  $\beta$ -structure, the N-terminus region behaves very similarly at the different pH values and does not seem to be significantly affected by pH. This region may have as much as

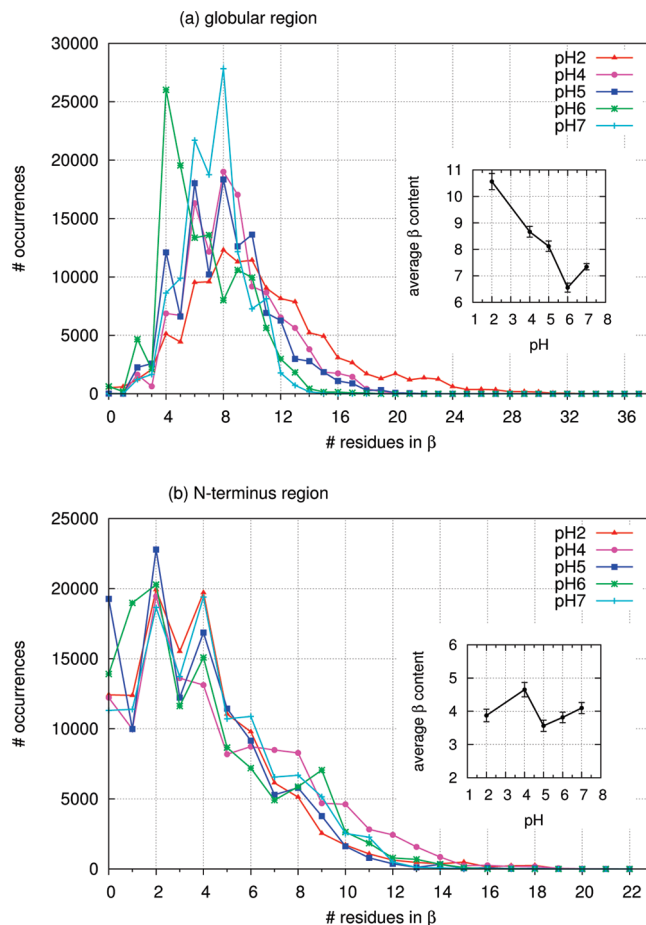


**Figure 8.** Histograms of the  $\beta$  content at each pH in (a) the globular region (125–228) and (b) the N-terminus region (90–124). The insets show the corresponding average number of residues in  $\beta$  at each pH.

22 residues in  $\beta$ -structure but the main peaks correspond to 2, 4, and 0 residues in  $\beta$ . At all pH values, there is on average around 4 residues in  $\beta$  in this region.

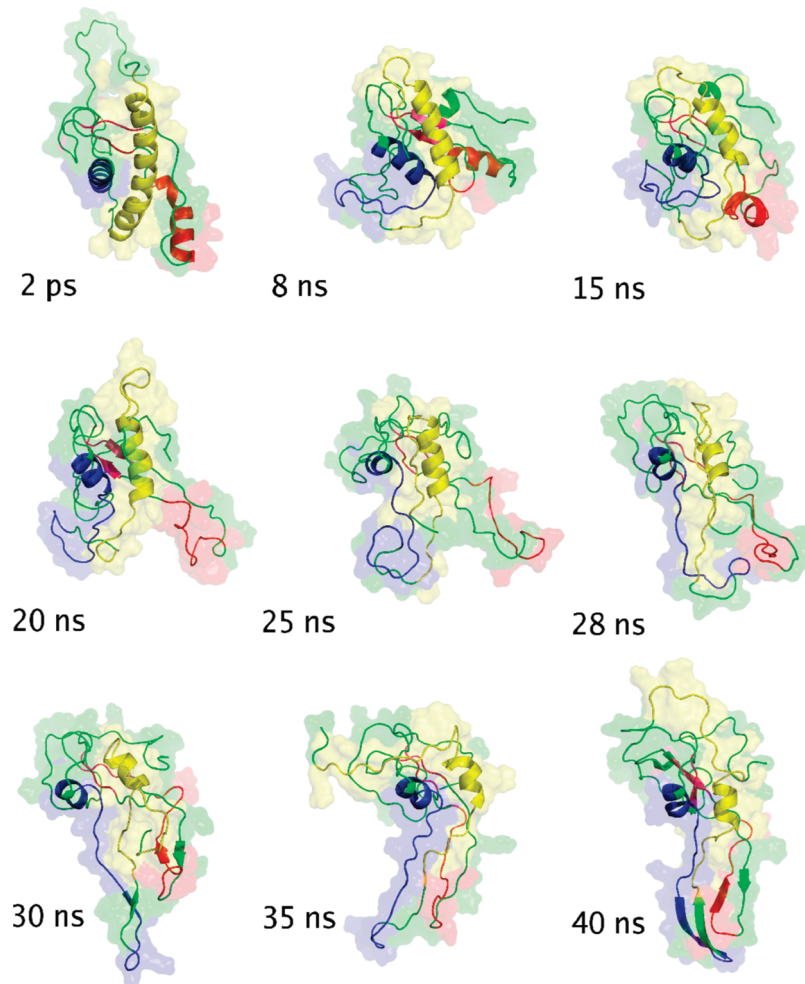


**Figure 9.** New  $\beta$ -sheet forming across time in one of the simulations at pH 2. See the color code in Figure 4. The secondary structure representation is according to the criteria used by PyMOL 0.99 (<http://www.pymol.org>), the program used here for molecular representation.

**Formation of a Stable  $\beta$ -Rich Structure.** New  $\beta$ -structure was frequently observed at low pH in the regions whose average structure and fluctuations depend the most on pH, namely, the segments 135–155 and 185–200 (Figures 4 and 5). At least one of these segments forms transient  $\beta$ -structure (for at least 1 ns) in 11 of the simulations at pH 2 and in 8 of the simulations at pH 4. However, the simultaneous formation of more extensive  $\beta$ -structure in both segments was observed only in one of the simulations at pH 2, leading to its significant increase in a seemingly cooperative way and resulting in a persistent  $\beta$ -rich structure. Figure 9 shows the conformational changes occurring across time in this simulation (movie available in Supporting Information). First, there is a progressive loss of helicity in the regions corresponding to HA, the C-terminus of HB and the N-terminus of HC (<25 ns). Then, after an alignment of these unwound regions (28 ns),  $\beta$ -sheet begins to form (30 ns) in two places: region 138–140 + 148–150, including part of former HA, and region 184–203, including the C-terminus of former HB. The central part of HC and the N-terminus of HB remain intact, most likely due to the stabilization effect of the disulfide bridge present in those regions. Also the original  $\beta$ -sheet is maintained though it loses some structure. The C-terminus of HC also unwinds at the beginning of the simulation. In Figure 10 we can see in more detail the residues involved in the formation of new  $\beta$ -structure. For instance, we can see that also region 120–122, in the N-terminus region, formed  $\beta$ -sheet. This  $\beta$ -strand pairs with the N-terminus of  $\beta$ 1, that gained two residues. The remaining part of  $\beta$ 1 continues to pair with  $\beta$ 2.

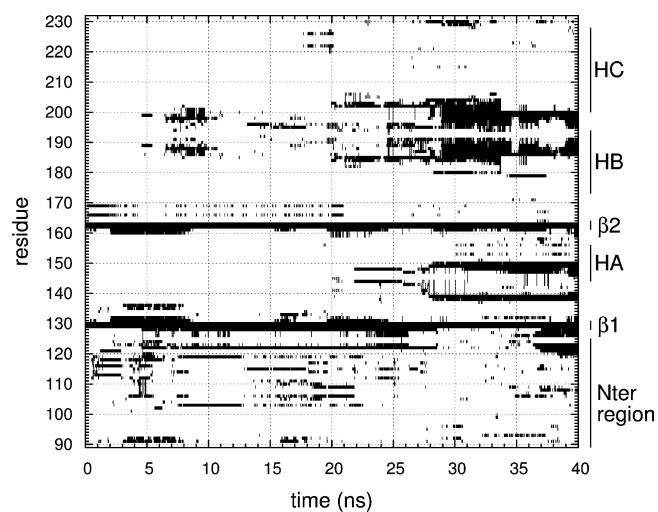


**Figure 10.** New  $\beta$ -sheet forming across time in one of the simulations at pH 2. The residues with  $\beta$ -structure at each instant are shown in black. Nter, N-terminus.

The rest of the N-terminus transiently forms  $\beta$ -structure in some regions, but it does not suffer any significant transformation.

The structure formed in the last nanoseconds of the simulation (last image in Figure 9) is particularly striking, featuring a well organized new region with canonical  $\beta$ -sheets that are easily identified by the molecular visualization software. This structure

may correspond to an intermediate state in the PrP<sup>C</sup> to PrP<sup>Sc</sup> conversion process.

These results suggest that the  $\beta$ -structure transiently observed at low pH in segments 135–155 and 185–200 can become stabilized in a cooperative way, acting as a nucleation seed and leading to a more persistent  $\beta$ -rich form. So we propose that at low pH values PrP<sup>C</sup> converts into a  $\beta$ -sheet rich structure (not necessarily PrP<sup>Sc</sup>) through the initial reorganization of segments around 135–155 (HA up to  $\beta$ 1) and 185–200 (C-terminus of HB up to HC).

## Discussion

As stated in the Introduction, most reported MD simulations of PrP only detected small structural changes, despite the use of the most varied ways of creating instability. This may be due to the small simulation times and small number of replicates used, but also to the use of lattice methods to treat long-range electrostatics.<sup>18,30,33,35,38,68</sup> Although a lattice method produced higher structural stabilization of PrP than a cutoff method,<sup>68</sup> several authors have argued that lattice methods can overstabilize the structures,<sup>43,69–71</sup> including PrP's.<sup>30</sup> In this work, we were able to observe important conformational changes in response to pH. This may be largely due to the extensive sampling obtained from the number of replicates and simulation time (which amounted to a total of 2.04  $\mu$ s). We also used the generalized reaction field method<sup>58</sup> to treat long-range electrostatics, avoiding the possible overstabilizing effect of the lattice methods.

It has been proven experimentally that human PrP 90–231 can form  $\beta$ -rich amyloid fibrils under acidic conditions.<sup>25,26,72</sup> This transition can occur in the absence of any denaturant despite being very slow (taking about 10 days to achieve the maximum fibril growth).<sup>5</sup> Circular dichroism experiments performed in the presence of denaturant allowed the observation of an acid-induced gradual transition of huPrP spectra from one typical of a helix-rich structure to one typical of a structure rich in  $\beta$ -sheet.<sup>15,24</sup> Our simulations are in good agreement with these observations, since the helix content decreased with low pH while the formation of new  $\beta$ -structure seemed to be favored. Most of our simulations at low pH exhibited the transient formation of new localized  $\beta$ -structure, which became persistent in only one simulation at pH 2, suggesting that the formation of a more stable  $\beta$ -rich structure is a rare and slow event. Several studies have also observed the existence of different types of soluble intermediates in the process of amyloid fibril formation, from partially folded to  $\beta$  type.<sup>28,73,74</sup> The gradual loss of helix content and concomitant formation of  $\beta$ -structure at low pH may account for these intermediates. In particular, the  $\beta$ -enrichment may be preceded by a helix-depleted partially folded structure, as observed in the simulation just mentioned, where the formation of new  $\beta$ -structure occurred after the unwinding of HA and part of HB and HC.

As mentioned in the Introduction, the 90–125 region of PrP has been thought to rearrange in the scrapie form. In fact, the existing models of PrP<sup>Sc</sup> fibrils<sup>34,75</sup> propose that the N-terminus reorganizes while at least the two last helices remain intact. Supporting these models is the finding that a peptide containing the 23–144 portion of human PrP can form amyloid fibrils.<sup>76</sup> Contradicting this theory is recent work of Surewicz and co-workers,<sup>5,72</sup> who by use of site-directed spin labeling and electron paramagnetic resonance spectroscopy were able to observe the formation of  $\beta$ -structure in the 160–220 region of the PrP core. The authors also observe<sup>72</sup> that the reduced protease K resistance of the synthetic fibrils compared with the

brain-derived ones suggest some rearrangement outside that region, which is not recreated in the experimental conditions. In addition, PrP 121–231 (without the N-terminus region) is able of forming  $\beta$ -structure<sup>24</sup> and the reorganization of the C-terminus core has been suggested by several NMR studies.<sup>16,27,28</sup> In our simulations we observe that the N-terminus region is very flexible and its structure is not affected by pH. Because it can transiently form  $\beta$ -structure, it is possible that this segment may acquire stable structure by forming  $\beta$ -sheets with pre-existing strands in the rearranged core of the protein (e.g., the elongated  $\beta$ 1 strand, Figure 10). Our results suggest that rearrangements occur in the regions HA up to  $\beta$ 1 and C-terminus of HB up to HC. These were the regions where the average structure and fluctuations depended the most on pH and where new  $\beta$ -sheet was observed. Our results also suggest that these structural changes may be largely triggered by the protonation of His187 and a consequent loss of interaction between the subdomains  $\beta$ 1 + HA +  $\beta$ 2 and HB + HC. Therefore, our results are consistent with the several works that suggested the C-terminus core as the region of major structural rearrangement.

This is the first time that the formation of new and persistent  $\beta$ -sheet in the globular core of human PrP 90–231, at physiological temperature, is observed in MD simulations. The  $\beta$ -rich structure formed may be an intermediate in the process of PrP<sup>Sc</sup> formation, suggesting that misfolding can precede aggregation. This observation shows that PrP can form a  $\beta$ -rich structure at low pH in the absence of a PrP template, a membrane, or protein X (a hypothetical auxiliary protein that was suggested to facilitate the conversion to the scrapie form<sup>77</sup>). We propose that low pH can by itself induce the misfolding of PrP<sup>C</sup> into a  $\beta$ -rich form, characterized by the reorganization of regions around 135–155 (HA up to  $\beta$ 1) and 185–200 (C-terminus of HB up to HC).

## Conclusions

In conclusion, our results support the theory that spontaneous conversion of PrP<sup>C</sup> to PrP<sup>Sc</sup> occur in the endocytic pathway induced by low pH. Obviously that there are several factors in vivo that are difficult to introduce in the standard experiments, such as glycosylation and Cu<sup>2+</sup> binding,<sup>7–9</sup> though they can affect the behavior of PrP. Nonetheless, our results were capable of reproducing what was observed in vitro, showing that constant-pH MD simulations are a reliable tool to study pH-induced conformational changes. Our main results and conclusions are summarized as follows.

(1) We present a titration curve and pK<sub>a</sub> calculations of the titrable sites at acidic pH. Unfortunately, there are no experimental results to compare with.

(2) His187 has a particularly low pK<sub>a</sub>, and it is located in a region of PrP that can suffer a conformational rearrangement at low pH. Its protonation may play an important role in PrP misfolding by weakening the interaction between subdomains  $\beta$ 1 + HA +  $\beta$ 2 and HB + HC.

(3) We observed a strong conformational pH-dependence. In particular, the helix content decreases and the  $\beta$  content increases toward acidic pH, in agreement with circular dichroism studies.<sup>15,24</sup>

(4) The pH-dependent conformational changes occur on the C-terminus core that also exhibits a pH-dependent plasticity. The N-terminus region is flexible, transiently forming  $\beta$ -structure, and does not seem to vary with pH.

(5) The regions with the highest rmsf are: HA up to  $\beta$ 1, C-terminus of HB up to HC, C-terminus of HC, the N-terminus region, and the loop between  $\beta$ 2 and HB. The most stable structural elements (smaller rmsf) are: N-terminus of HB, central

part of HC, and the β-sheet ( $\beta_1 + \beta_2$ ). These observations are in agreement with experimental data.<sup>10,64,65</sup>

(6) The regions whose fluctuations are pH-dependent and where restructuring at acidic pH occurs are: HA up to  $\beta_1$  (135–155) and C-terminus of HB up to HC (185–200).

(7) Human PrP 90–231 is able of forming a persistent β-rich intermediate at low pH, in the absence of a membrane or other proteins (PrP<sup>C</sup>, PrP<sup>Sc</sup>, or protein X). This means that the initial steps of the conformational change may occur prior to aggregation. Nonetheless, this is a rare event even at very low pH.

**Acknowledgment.** We thank Cláudio M. Soares for fruitful discussions. We acknowledge financial support from Fundação para a Ciência e a Tecnologia, Portugal, through Grants SFRH/BD/23506/2005, SFRH/BPD/29358/2006, and PTDC/QUI-BIQ/105238/2008.

**Supporting Information Available:** Figure showing the residues with which His187 interacts at the different pH values, and film of one of the simulations of human PrP at pH 2, showing the formation of a stable β-rich structure. This material is available free of charge via the Internet at <http://pubs.acs.org/>.

## References and Notes

- (1) Perutz, M. F. *Science* **1978**, *201*, 1187–1191.
- (2) Ma, K.; Clancy, E. L.; Zhang, Y.; Ray, D. G.; Wollenberg, K.; Zagorski, M. G. *J. Am. Chem. Soc.* **1999**, *121*, 8698–8706.
- (3) Uversky, V. N.; Li, J.; Fink, A. L. *J. Biol. Chem.* **2001**, *276*, 10737–10744.
- (4) Chiti, F.; Dobson, C. M. *Annu. Rev. Biochem.* **2006**, *75*, 333–366.
- (5) Cobb, N. J.; Apetri, A. C.; Surewicz, W. K. *J. Biol. Chem.* **2008**, *283*, 34704–34711.
- (6) Machuqueiro, M.; Baptista, A. M. *J. Phys. Chem. B* **2006**, *110*, 2927–2933.
- (7) Prusiner, S. B. *Proc. Natl. Acad. Sci. U.S.A.* **1998**, *95*, 13363–13383.
- (8) Abid, K.; Soto, C. *Cell. Mol. Life Sci.* **2006**, *63*, 2342–2351.
- (9) Cobb, N. J.; Surewicz, W. K. *Biochemistry* **2009**, *48*, 2574–2585.
- (10) Calzolai, L.; Zahn, R. *J. Biol. Chem.* **2003**, *278*, 35592–35596.
- (11) Pan, K.-M.; Baldwin, M.; Nguyen, J.; Gasset, M.; Serban, A.; Groth, D.; Mehlhorn, I.; Huang, Z.; Fletterick, R. J.; Cohen, F. E. *Proc. Natl. Acad. Sci. U.S.A.* **1993**, *90*, 10962–10966.
- (12) Caughey, B. W.; Dong, A.; Bhat, K. S.; Ernst, D.; Hayes, S. F.; Caughey, W. S. *Biochemistry* **1991**, *30*, 7672–7680.
- (13) Gasset, M.; Baldwin, M. A.; Fletterick, R. J.; Prusiner, S. B. *Proc. Natl. Acad. Sci. U.S.A.* **1993**, *90*, 1–5.
- (14) Weissmann, C. *Cell* **2005**, *122*, 165–168.
- (15) Swietnicki, W.; Petersen, R.; Gambetti, P.; Surewicz, W. K. *J. Biol. Chem.* **1997**, *272*, 27517–27520.
- (16) Jackson, G. S.; Hosszu, L. L. P.; Power, A.; Hill, A. F.; Kenney, J.; Saibil, H.; Craven, C. J.; Walther, J. P.; Clarke, A. R.; Collinge, J. *Science* **1999**, *283*, 1935–1937.
- (17) DeMarco, M. L.; Daggett, V. *C. R. Biol.* **2005**, *328*, 847–862.
- (18) Langella, E.; Imrota, R.; Barone, V. *Biophys. J.* **2004**, *87*, 3623–3632.
- (19) Shyng, S.-L.; Huber, M. T.; Harris, D. A. *J. Biol. Chem.* **1993**, *268*, 15922–15928.
- (20) Magalhães, A. C.; Silva, J. A.; Lee, K. S.; Martins, V. R.; Prado, V. F.; Ferguson, S. S. G.; Gomez, M. V.; Brentani, R. R.; Prado, M. A. M. *J. Biol. Chem.* **2002**, *277*, 33311–33318.
- (21) Taraboulos, A.; Raeber, A. J.; Borchelt, D. R.; Serban, D.; Prusiner, S. B. *Mol. Biol. Cell* **1992**, *3*, 851–863.
- (22) Borchelt, D. R.; Taraboulos, A.; Prusiner, S. B. *J. Biol. Chem.* **1992**, *267*, 16188–16199.
- (23) Arnold, J. E.; Tippler, C.; Laszlo, L.; Hope, J.; Landon, M.; Mayer, R. J. *J. Pathol.* **1995**, *176*, 403–411.
- (24) Horneemann, S.; Glockshuber, R. *Proc. Natl. Acad. Sci. U.S.A.* **1998**, *95*, 6010–6014.
- (25) Swietnicki, W.; Morillas, M.; Chen, S. G.; Gambetti, P.; Surewicz, W. K. *Biochemistry* **2000**, *39*, 424–431.
- (26) Morillas, M.; Vanik, D. L.; Surewicz, W. K. *Biochemistry* **2001**, *40*, 6982–6987.
- (27) O'Sullivan, D. B. D.; Jones, C. E.; Abdelraheim, S. R.; Thompsett, A. R.; Brazier, M. W.; Toms, H.; Brown, D. R.; Viles, J. H. *Biochem. J.* **2007**, *401*, 533–540.
- (28) Gerber, R.; Tahiri-Alaoui, A.; Hore, P. J.; James, W. *Protein Sci.* **2008**, *17*, 537–544.
- (29) Zahn, R.; Liu, A.; Lührs, T.; Riek, R.; von Schroetter, C.; García, F. L.; Billeter, M.; Calzolai, L.; Wider, G.; Wüthrich, K. *Proc. Natl. Acad. Sci. U.S.A.* **2000**, *97*, 145–150.
- (30) El-Bastawissy, E.; Knaggs, M. H.; Gilbert, I. H. *J. Mol. Graph. Model.* **2001**, *20*, 145–154.
- (31) Gu, W.; Wang, T.; Zhu, J.; Shi, Y.; Liu, H. *Biophys. Chem.* **2003**, *104*, 79–94.
- (32) Shamsir, M. S.; Dalby, A. R. *Proteins* **2005**, *59*, 275–290.
- (33) Colacino, S.; Tiana, G.; Broglia, R. A.; Colombo, G. *Proteins* **2006**, *62*, 698–707.
- (34) DeMarco, M. L.; Daggett, V. *Proc. Natl. Acad. Sci. U.S.A.* **2004**, *101*, 2293–2298.
- (35) Barducci, A.; Chelli, R.; Procacci, P.; Schettino, V. *Biophys. J.* **2005**, *88*, 1334–1343.
- (36) Alonso, D. O. V.; DeArmond, S. J.; Cohen, F. E.; Daggett, V. *Proc. Natl. Acad. Sci. U.S.A.* **2001**, *98*, 2985–2989.
- (37) Alonso, D. O. V.; An, C.; Daggett, V. *Philos. Trans. R. Soc. Lond. A* **2002**, *360*, 1165–1178.
- (38) Langella, E.; Imrota, R.; Crescenzi, O.; Barone, V. *Proteins* **2006**, *64*, 167–177.
- (39) DeMarco, M. L.; Daggett, V. *Biochemistry* **2007**, *46*, 3045–3054.
- (40) Peretz, D.; Williamson, R. A.; Matsunaga, Y.; Serban, H.; Pinilla, C.; Bastidas, R. B.; Rozenshteyn, R.; James, T. L.; Houghten, R. A.; Cohen, F. E.; Prusiner, S. B.; Burton, D. R. *J. Mol. Biol.* **1997**, *273*, 614–622.
- (41) Baptista, A. M.; Teixeira, V. H.; Soares, C. M. *J. Chem. Phys.* **2002**, *117*, 4184–4200.
- (42) Machuqueiro, M.; Baptista, A. M. *Biophys. J.* **2007**, *92*, 1836–1845.
- (43) Machuqueiro, M.; Baptista, A. M. *Proteins* **2008**, *72*, 289–298.
- (44) Machuqueiro, M.; Baptista, A. M. *J. Am. Chem. Soc.* **2009**, *131*, 12586–12594.
- (45) Lee, R. J.; Wang, S.; Low, P. S. *Biochim. Biophys. Acta* **1996**, *1312*, 237–242.
- (46) James, T. L.; Liu, H.; Ulyanov, N. B.; Farr-Jones, S.; Zhang, H.; Donnes, D. G.; Kaneko, K.; Groth, D.; Mehlhorn, I.; Prusiner, S. B.; Cohen, F. E. *Proc. Natl. Acad. Sci. U.S.A.* **1997**, *94*, 10086–10091.
- (47) Kabsch, W.; Sander, C. *Biopolymers* **1983**, *22*, 2577–2637.
- (48) Baptista, A. M.; Soares, C. M. *J. Phys. Chem. B* **2001**, *105*, 293–309.
- (49) Bashford, D.; Gerwert, K. *J. Mol. Biol.* **1992**, *224*, 473–486.
- (50) van Gunsteren, W. F.; Billeter, S. R.; Eising, A. A.; Hünenberger, P. H.; Krüger, P.; Mark, A. E.; Scott, W. R. P.; Tironi, I. G. *Biomolecular simulation: the GROMOS96 manual and user guide*; vdf Hochschulverlag AG an der ETH Zürich: Zurich, Switzerland, 1996.
- (51) Gilson, M. K.; Sharp, K. A.; Honig, B. H. *J. Comput. Chem.* **1987**, *9*, 327–335.
- (52) Baptista, A. M.; Martel, P. J.; Soares, C. M. *Biophys. J.* **1999**, *76*, 2978–2998.
- (53) Metropolis, N.; Rosenbluth, A. W.; Rosenbluth, M. N.; Teller, A. H.; Teller, E. *J. Chem. Phys.* **1953**, *21*, 1087–1092.
- (54) Lindahl, E.; Hess, B.; van der Spoel, D. *J. Mol. Model.* **2001**, *7*, 306–317.
- (55) van der Spoel, D.; Lindahl, E.; Hess, B.; Groenhof, G.; Mark, A. E.; Berendsen, H. J. C. *J. Comput. Chem.* **2005**, *26*, 1701–1718.
- (56) Oostenbrink, C.; Villa, A.; Mark, A. E.; van Gunsteren, W. F. *J. Comput. Chem.* **2004**, *25*, 1656–1676.
- (57) Hermans, J.; Berendsen, H. J. C.; van Gunsteren, W. F.; Postma, J. P. M. *Biopolymers* **1984**, *23*, 1513–1518.
- (58) Tironi, I. G.; Sperb, R.; Smith, P. E.; van Gunsteren, W. F. *J. Chem. Phys.* **1995**, *102*, 5451–5459.
- (59) Berendsen, H. J. C.; Postma, J. P. M.; van Gunsteren, W. F.; DiNola, A.; Haak, J. R. *J. Chem. Phys.* **1984**, *81*, 3684–3690.
- (60) Hess, B.; Bekker, H.; Berendsen, H. J. C.; Fraaije, J. G. E. M. *J. Comput. Chem.* **1997**, *18*, 1463–1472.
- (61) Allen, M. P.; Tildesley, D. J. *Computer Simulation of Liquids*; Oxford University Press: Oxford, 1987.
- (62) Press, W. H.; Teukolsky, S. A.; Vetterling, W. T.; Flannery, B. P. *Numerical recipes in C: the art of scientific computing*, 2nd ed.; Cambridge University Press: New York, 1992.
- (63) Colucci, M.; Moleres, F. J.; Xie, Z.-L.; Ray-Chaudhury, A.; Gutti, S.; Butefisch, C. M.; Cervenakova, L.; Wang, W.; Goldfarb, L. G.; Kong, Q.; Ghetti, B.; Chen, S. G.; Gambetti, P. *J. Neuropathol. Exp. Neurol.* **2006**, *65*, 642–651.
- (64) Viles, J. H.; Donne, D.; Kroon, G.; Prusiner, S. B.; Cohen, F. E.; Dyson, H. J.; Wright, P. E. *Biochemistry* **2001**, *40*, 2743–2753.
- (65) Soto, C. *Proc. Natl. Acad. Sci. U.S.A.* **2009**, *106*, 10–11.
- (66) Schwarzsinger, S.; Horn, A. H. C.; Ziegler, J.; Sticht, H. *J. Biomol. Struct. Dyn.* **2006**, *23*, 581–590.
- (67) De Simone, A.; Zagari, A.; Derreumaux, P. *Biophys. J.* **2007**, *93*, 1284–1292.
- (68) Zuegg, J.; Gready, J. E. *Biochemistry* **1999**, *38*, 13862–13876.

- (69) Hünenberger, P. H.; McCammon, J. A. *Biophys. Chem.* **1999**, *78*, 69–88.
- (70) Kastenholz, M. A.; Hünenberger, P. H. *J. Phys. Chem. B* **2004**, *108*, 774–788.
- (71) Lins, R. D.; Röthlisberger, U. *J. Chem. Theory Comput.* **2006**, *2*, 246–250.
- (72) Cobb, N. J.; Sönnichsen, F. D.; Mchaourab, H.; Surewicz, W. K. *Proc. Natl. Acad. Sci. U. S. A.* **2007**, *104*, 18946–18951.
- (73) Apetrii, A. C.; Surewicz, W. K. *J. Biol. Chem.* **2002**, *277*, 44589–44592.
- (74) Kuwata, K.; Li, H.; Yamada, H.; Legname, G.; Prusiner, S. B.; Akasaka, K.; James, T. L. *Biochemistry* **2002**, *41*, 12277–12283.
- (75) Govaerts, C.; Wille, H.; Prusiner, S. B.; Cohen, F. E. *Proc. Natl. Acad. Sci. U. S. A.* **2004**, *101*, 8342–8347.
- (76) Kundu, B.; Maiti, N. R.; Jones, E. M.; Surewicz, K. A.; Vanik, D. L.; Surewicz, W. K. *Proc. Natl. Acad. Sci. U. S. A.* **2003**, *100*, 12069–12074.
- (77) Telling, G. C.; Scott, M.; Mastrianni, J.; Gabizon, R.; Torchia, M.; Cohen, F. E.; DeArmond, S. J.; Prusiner, S. B. *Cell* **1995**, *83*, 79–90.

JP104753T